

Mode-II Fracture in E-glass–polyester Composite

ANDRÁS SZEKRÉNYES* AND JÓZSEF UJ

*Department of Applied Mechanics
Budapest University of Technology and Economics
Budapest, P.O. Box 11, H-1521, Hungary*

(Received July 26, 2004)
(Accepted November 8, 2004)

ABSTRACT: In this work a novel beam analysis of the end-loaded split (ELS) and over-notched flexure (ONF) specimens are presented. New compliance and strain energy release rate equations are developed incorporating crack tip deformation and transverse shear analysis. The Saint Venant effect at the clamped end of the ELS specimen is also considered. Unidirectional glass–polyester specimens are manufactured and experimental (initiation and propagation) tests are performed to confirm the theoretical models. The experimental data is evaluated by means of four reduction techniques: the exact beam theory, virtual crack closure technique, compliance calibration method, and direct beam theory. It is shown that the results by the four methods agree quite closely; however, the compliance calibration method is not recommended for initiation data reduction in the case of the ONF specimen. The ELS specimens suffer from relatively large displacements. Thus, propagation tests are not possible to be performed. The ONF test seems to be a better tool to evaluate the mode-II toughness of composite materials with low flexural modulus.

KEY WORDS: delamination, strain energy release rate, crack tip deformation, transverse shear, end-loaded split, over-notched flexure.

INTRODUCTION

THE INCREASING APPLICATION of composite materials in the aircraft and automobile industry encouraged the researchers to study the fracture behavior of composite systems. Great attention has been focused in the last decade on the investigation of the mode-II interlaminar fracture.

The most popular specimen geometries are the end-notched flexure (ENF) and the four-point bend end-notched flexure (4ENF) specimens. The mode-II fracture in these coupons was discussed by many authors from the theoretical and experimental points of view [1–6]. A remarkable study was performed on carbon fiber-reinforced ENF and 4ENF systems

*Author to whom correspondence should be addressed. E-mail: szeki@mm.bme.hu

by Schuecker and Davidson [1]. It was shown that these two tests give the same fracture toughness values if the crack length and the compliance are measured accurately. The stabilized end-notched flexure (SENF) specimen was developed [7] to overcome the problem of instability in the ENF specimen. Another candidate for mode-II fracture investigation is the end-loaded split (ELS) specimen, which was studied in detail by Hashemi et al. [8,9] and Wang et al. [10]. The over-notched flexure (ONF) specimen was applied by other researchers [11,12]. Finally the tapered end-notched flexure (TENF) specimen should be mentioned, which is an efficient way to investigate the mode-II fracture in composites [13,14].

According to this short review, six specimens are available for mode-II fracture investigation. The ENF specimen is suitable only to determine the initiation toughness; crack stability restricts the available crack length range. The SENF configuration requires additional equipment compared to the ENF one. The usage of the ELS specimen is limited by large displacements and again by crack stability, but it is possible to perform propagation tests with it. The 4ENF specimen requires a slightly complex loading system, but it eliminates the transverse shear effect and is suitable to measure the propagation toughness. In the TENF specimen, the geometry is slightly difficult compared to the traditional ENF one; however, it was shown that in the case of proper specimen design, the compliance rate change is independent of the crack length [13,14]. The ONF specimen seems to be the simplest alternative, i.e., we need only a three-point bending setup, no large displacement occurs and (as will be shown later) the stable crack propagation is guaranteed at any crack length.

Within the scope of linear elastic fracture mechanics (LEFM), the fracture specimens are treated as slender beams. The solutions are essentially based on simple beam theory; however, this can be improved using other theories. Ozdil et al. [15] applied the Timoshenko beam theory for angle-ply laminate ENF specimen. The transverse shear effect was found to be insignificant. Carlsson et al. [16] introduced a correction for the strain energy release rate (SERR) incorporating transverse shear analysis; however, only a small improvement was made compared to the simple beam theory solution. The elastic foundation models were successfully applied for mode-I fracture problems [17,18]. Hence, the researchers tried to develop similar models for mode-II fracture specimens also. An improved analysis was performed by Chatterje [19] for the ENF specimen. The solution was in good agreement with previous finite element (FE) results. Later, Ding and Kortschot [20] applied tangential springs along the midplane of the ENF specimen. Unfortunately, their model was too complicated and could not be applied directly. Wang and Qiao [21] provided the simplest and most practical solution for the ENF specimen. The results of their analysis (called crack tip deformation) were in excellent agreement with previous FE studies. Later, the crack tip deformation theory, together with the elastic foundation model was used to obtain generalized solutions for bimaterial interfaces [22,23].

The energy release rate may be obtained in closed form by a combined beam theory–FE-based analysis. In this respect, the works by Wang and Williams [24] and Bao et al. [25] are noteworthy.

The objective of our work is to develop improved solutions for the compliance and the energy release rate of the ELS and ONF coupons. The analyses by Ozdil et al. [16], Olsson [17], and Wang and Qiao [21] are incorporated. From other perspectives, relatively small amount of experimental results were found in the literature as regarding the glass-fiber-reinforced ELS and, especially the ONF specimens. The current work seeks

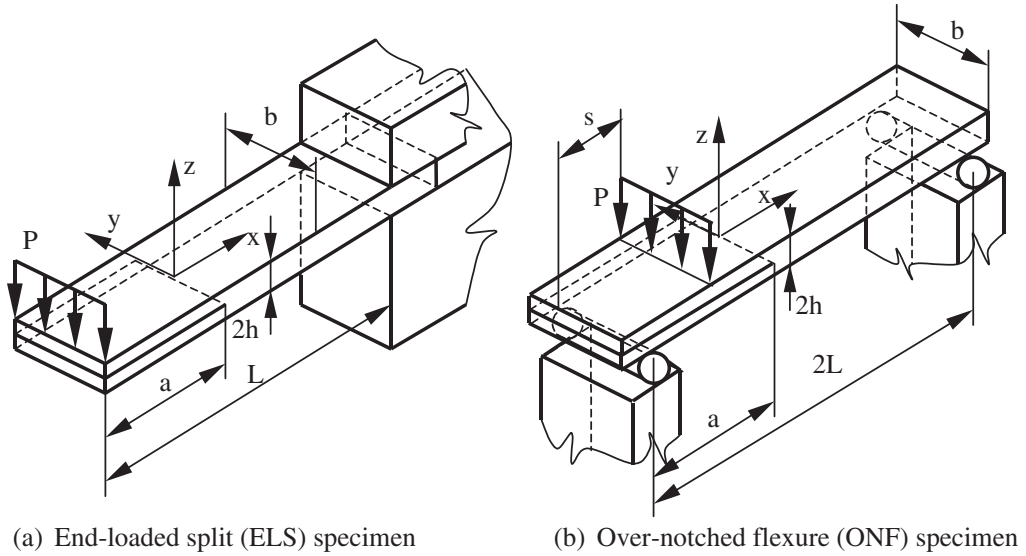


Figure 1. Mode-II fracture specimens.

to address this void. The mode-II fracture specimens are illustrated in Figure 1. Our choice can further be explained by the facts that these specimens are suitable for propagation tests and require simpler experimental equipment than the 4ENF test. Moreover, the location of load introduction and constraints of the ELS and ONF coupons are essentially different. Comparison between their results may be useful. The test coupons are analyzed by using linear beam theories, the FE method, and experiments.

BEAM ANALYSIS

The beam analysis section primarily investigates the ELS specimen, but the analysis will be extended to the ONF specimen, also. The analysis of Wang and Qiao [21] is closely followed. In Figure 2(a), the model of the ELS specimen is subjected to end loading P (subproblem one), while the subproblem two in Figure 2(b) represents a beam with a shear traction along the neutral plane of the upper specimen arm. Due to skew symmetry, only the upper half of the beam is analyzed. We solve the problem by superposing the results of the two subproblems in Figure 2, which leads to the complete solution.

Euler–Bernoulli and Timoshenko Beam Theory

The solution of problem (a) in Figure 2 including transverse shear effect can be obtained based on previous works [16,21]. Thus, the compliance of the ELS specimen becomes:

$$C = \frac{3a^3 + L^3}{2bh^3E_{11}} + \frac{L}{2bhkG_{13}}, \quad (1)$$

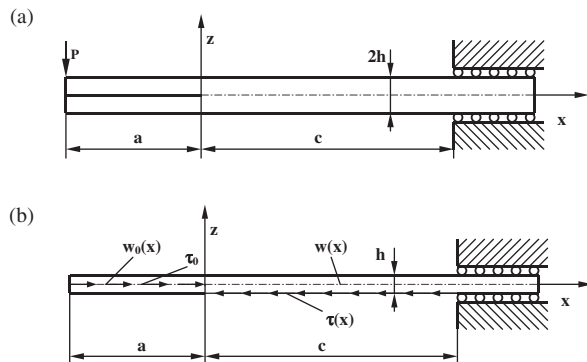


Figure 2. For the beam analysis of the ELS specimen.

where a is the crack length, L is the specimen length, b is the width, h is half of the thickness (refer to Figure 1), E_{11} is the flexural modulus, G_{13} is the shear modulus, and $k = 5/6$ is the shear correction factor.

Crack Tip Deformation Analysis

In this section we analyze only problem (b) in Figure 2 by following the work of Wang and Qiao [21]. Note that $w(x)$ is the deflection function of the uncracked region, while $w_0(x)$ is the deflection function of the cracked portion of the beam. The shear stress, τ_0 can be calculated on the basis of strength of materials analysis. Its magnitude is:

$$\tau_0 = \frac{3P}{4bh}, \quad (2)$$

where P is the applied load (Figure 2(a)). The relationships of internal forces and stresses are:

$$\frac{dN}{dx} = b\tau, \quad \frac{dM}{dx} = -\frac{h}{2}b\tau, \quad (3)$$

where N is the normal force and M is the bending moment. We use the following constitutive equations:

$$\frac{d^2w}{dx^2} = -\frac{M}{I_y E_{11}}, \quad \frac{du}{dx} = -\frac{N}{E_{11}bh}, \quad (4)$$

where I_y is the second-order moment of inertia. The longitudinal displacement along the neutral plane of the uncracked region should be zero, consequently we have:

$$u(x) = -\frac{1}{bhE_{11}} \int N dx + K\tau - \frac{h}{2} \frac{dw}{dx} = 0, \quad (5)$$

where K is the shear compliance:

$$K = \frac{h}{3\lambda G_{13}}. \quad (6)$$

In Equation (6), λ is the modification factor due to orthotropy. After differentiating Equation (5) twice we obtain:

$$K \frac{d^2 \tau}{dx^2} - \frac{1}{bhE_{11}} \frac{dN}{dx} - \frac{h}{2} \frac{d^3 w}{dx^3} = 0. \quad (7)$$

Differentiating the first expression in Equation (4) and combining it with Equations (3) and (7) one may obtain the governing differential equation with respect to the shear stress:

$$\frac{d^2 \tau}{dx^2} - \alpha^2 \tau = 0, \quad \alpha = \left(\frac{12\lambda G_{13}}{E_{11} h^2} \right)^{1/2}. \quad (8)$$

The solution of the differential equation is:

$$\tau(x) = c_1 e^{-\alpha x} + c_2 e^{\alpha x}. \quad (9)$$

The term after c_2 is very small and can be neglected. The longitudinal forces must vanish along the full length of the specimen [21]. This condition allows for the determination of c_1 . The approximate solution of Equation (8) becomes:

$$\tau(x) = -\frac{3}{4} \frac{P}{bh} \alpha \cdot a e^{-\alpha x}. \quad (10)$$

The bending moment function yields by integrating the shear stress along the uncracked region. From Equation (4), the deflection of the uncracked part is:

$$w(x) = -\frac{3}{8} \frac{Pa}{I_y E_{11} \alpha^2} e^{-\alpha x} + d_1 x + d_2, \quad I_y = \frac{bh^3}{12}. \quad (11)$$

Since the shear traction acts along the neutral plane of the cracked region, the deflection function can be obtained as:

$$w_0(x) = d_3 x + d_4. \quad (12)$$

In order to determine the four constant parameters (d_1 – d_4) we use the following boundary and matching conditions:

$$\begin{aligned} w(c) &= 0, & w'(c) &= 0, \\ w_0(0) &= w(0), & w'_0(0) &= w'(0). \end{aligned} \quad (13)$$

After simplification, the compliance of the beam in Figure 2(b) becomes:

$$C_{SH} = \frac{w_0(-a)}{P} = \frac{3}{8I_y E_{11}} \left[\frac{a}{\alpha^2} + \frac{a^2}{\alpha} \right]. \quad (14)$$

Wang and Qiao have found the best agreement with FE results in the case of $\lambda = 6$. Substituting α (Equation (8)) into Equation (14) we obtain:

$$C_{SH} = \frac{a^3}{2bh^3 E_{11}} \left[1.06 \left(\frac{h}{a} \right) \left(\frac{E_{11}}{G_{13}} \right)^{\frac{1}{2}} + 0.125 \left(\frac{h}{a} \right)^2 \left(\frac{E_{11}}{G_{13}} \right) \right]. \quad (15)$$

Saint Venant Effect

The problem of Saint Venant effect was analyzed by Olsson [17] for the double-cantilever beam (DCB) specimen. The Saint Venant effect is necessary to be considered due to the clamped end of the ELS coupon. Referring to Olsson's analysis, the compliance contribution has the following form in the case of the mode-II ELS specimen:

$$C_{SV} = \frac{3}{\pi} \frac{L^2}{2bh^2 E_{11}} \left(\frac{E_{11}}{G_{13}} \right)^{1/2}, \quad (16)$$

which is independent of the crack length, and (as shown later) does not provide any contribution to the SERR.

SUMMARY OF THE COMPLIANCE AND ENERGY RELEASE RATE ELS Specimen

Superposing Equations (1), (15), and (16) we obtain the compliance of the ELS specimen:

$$C^{\text{ELS}} = \frac{3a^3 + L^3}{2bh^3 E_{11}} + \frac{L}{2bhk G_{13}} + \frac{3}{\pi} \frac{L^2}{2bh^2 E_{11}} \left(\frac{E_{11}}{G_{13}} \right)^{1/2} + \frac{a^3}{2bh^3 E_{11}} \left[1.06 \left(\frac{h}{a} \right) \left(\frac{E_{11}}{G_{13}} \right)^{1/2} + 0.125 \left(\frac{h}{a} \right)^2 \left(\frac{E_{11}}{G_{13}} \right) \right]. \quad (17)$$

The mode-II SERR is given by the Irwin-Kies expression [16]:

$$G_{\text{II}} = \frac{P^2}{2b} \frac{dC}{da}. \quad (18)$$

The combination of Equations (17) and (18) results in:

$$G_{II}^{ELS} = \frac{9P^2 a^2}{4b^2 h^3 E_{11}} \left[1 + 0.236 \left(\frac{h}{a} \right) \left(\frac{E_{11}}{G_{13}} \right)^{1/2} + 0.014 \left(\frac{h}{a} \right)^2 \left(\frac{E_{11}}{G_{13}} \right) \right]. \quad (19)$$

ONF Specimen

Based on the analysis, equations similar to the aforementioned may be derived for the ONF specimen, also. The compliance is:

$$C^{ONF} = \frac{s^2 c^3}{8bh^3 E_{11} L^2} \left[1 + 4 \frac{a}{c} + 8 \frac{aL}{c^2} + 16 \frac{aL^2}{c^3} + 8 \frac{Ls(s-4L)}{c^3} \right] + \frac{s(2L-s)}{8bhkG_{13}L} + \frac{s^2 c^3}{8bh^3 E_{11} L^2} \left[1.06 \left(\frac{h}{c} \right) \left(\frac{E_{11}}{G_{13}} \right)^{1/2} + 0.125 \left(\frac{h}{c} \right)^2 \left(\frac{E_{11}}{G_{13}} \right) \right], \quad (20)$$

where L is half of the span length, s is the position of the applied load, and c is the length of the uncracked region ($2L - a$) (see Figure 1(b)). The first term is from Euler–Bernoulli beam theory, the second from Timoshenko beam theory, and the last one from crack tip deformation analysis. The mode-II strain energy release rate by using Equation (18) becomes:

$$G_{II}^{ONF} = \frac{9P^2 s^2 c^2}{16b^2 h^3 E_{11} L^2} \left[1 + 0.236 \left(\frac{h}{c} \right) \left(\frac{E_{11}}{G_{13}} \right)^{1/2} + 0.014 \left(\frac{h}{c} \right)^2 \left(\frac{E_{11}}{G_{13}} \right) \right]. \quad (21)$$

To the best of our knowledge, these equations are not yet published in the literature. In the following sections, we verify the derived equations by numerical models and experiments.

Crack Stability

The problem of crack stability was investigated by Carlsson et al. [16] for the ENF specimen and Davies et al. [26] for the ELS specimen. For the commonly assumed fixed grip condition, the SERR may be expressed as [15]:

$$G_{II} = \frac{\delta^2}{2bC^2} \frac{dC}{da}. \quad (22)$$

Stable crack propagation can be expected if dG_{II}/da is zero or negative. Differentiating Equation (22) with respect to the crack length yields:

$$\frac{dG_{II}}{da} = \frac{\delta^2}{2bC^2} \left(\frac{d^2 C}{da^2} - \frac{2}{C} \left(\frac{dC}{da} \right)^2 \right). \quad (23)$$

We consider only the first term in Equation (17). Substituting it into Equation (23) we obtain:

$$\frac{a}{L} \geq 0.55, \quad (24)$$

i.e., stable crack propagation in the ELS specimen may be expected if Equation (24) is satisfied. If we perform only the initiation tests, then Equation (24) can be ignored, since in this case we need the critical load and the deflection only at the point of fracture initiation. These may be determined experimentally at those crack lengths ($a < 0.55L$), which do not satisfy Equation (24).

For the ONF specimen, the result of the simple beam theory is the first term in Equation (20). Substituting it into Equation (23), and assuming that the right-hand side of Equation (23) is equal to zero, we obtain a fourth-order polynomial as a function of the crack length. The polynomial has four roots, of which two are real:

$$(a)_1 = 2L, \quad (a)_2 = \frac{1}{3}(144L^3 - 144sL^2 + 36Ls^2)^{1/3} + 2L. \quad (25)$$

Since s is always less than L it appears that we should consider only the first root. If $a \leq (a)_1$ then dG_{II}/da is zero or negative. On the other hand, it is obvious that a should always be higher than s but (as Equation (25) shows) should be less than $2L$. Thus, the requirement is:

$$s < a < 2L, \quad (26)$$

i.e., stable crack propagation may be expected at any crack length.

The Effect of Friction

The effect of friction in mode-II fracture specimens was investigated by Wang et al. [12]. The Coulomb-type friction model including frictional coefficients within $\mu = 0.25$ and 0.5 was adopted in their work. The developed beam and FE models indicated negligible effects induced by friction. In the case of $\mu = 0.25$, the energy release rate changes by only 3% due to friction between crack faces. We have found that this is close to a practical value [27]. As a consequence, the effect of friction on the SERR of both specimens was neglected in the current study.

FINITE ELEMENT ANALYSIS

The FE analysis was performed under plane strain condition to validate the beam theory-based equations. The specimens were meshed with linear PLANE2D elements using the commercial FE code COSMOS/M 2.0. The details of the FE model of the ELS specimen are demonstrated in Figure 3. For the ONF specimen, a similar FE model was developed. The material was assumed to be linear elastic with orthotropic material properties. The material properties and the model dimensions are given in the next section.

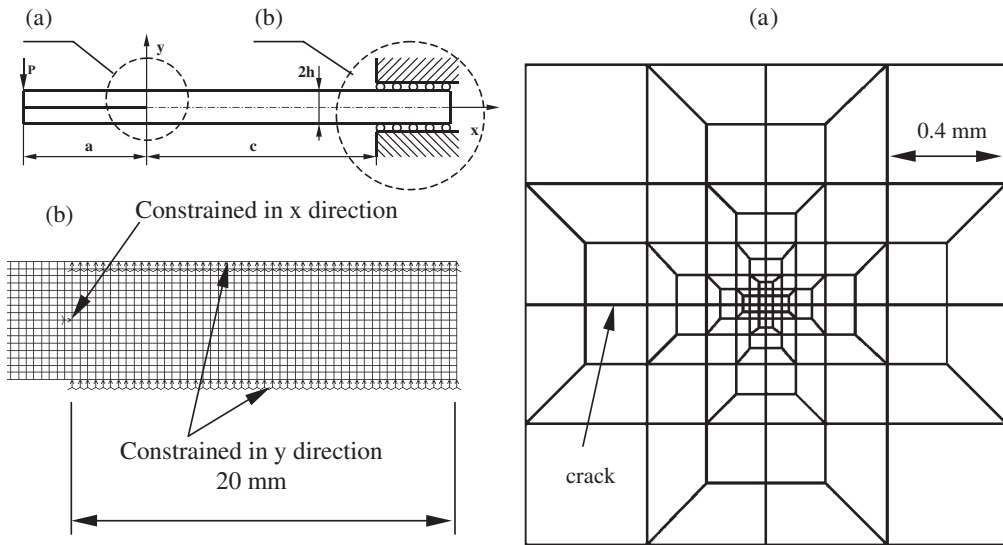


Figure 3. Details of the FE model of the ELS specimen. FE mesh around the crack tip (a) and details of the clamped end (b).

In order to prevent the penetration between the nodes along the crack faces, the same vertical displacements were imposed by using the command CPDOF. The specimens were loaded by concentrated forces, of which values were determined based on experimental initiation tests. The compliance ($C = \delta/P$, where δ is the deflection at the point of load application) of the specimens was used to validate the beam theory-based solutions. Moreover, the mode-II energy release rate (G_{II}) was calculated by means of the virtual crack closure technique (VCCT) [28]. At the crack tip a typical mesh (Figure 3(b)) as suggested by Davidson et al. [29] was constructed with singular elements. The finite crack extension was $\Delta a = 0.025$ mm.

EXPERIMENTS AND DATA REDUCTION

The constituent materials were procured from a native company (Novia Ltd). The properties of the E-glass fiber are $E = 70$ GPa and $\nu = 0.27$, while for the unsaturated polyester resin they are $E = 3.5$ GPa and $\nu = 0.35$. Both were considered as isotropic. The unidirectional ($[0^\circ]_{14}$) E-glass–polyester specimens with nominal thickness of $2h = 6.1$ mm, width of $b = 20$ mm, total length of 180 mm, and $V_f = 43\%$ were manufactured in a special pressure tool. A great advantage of this material is the transparency, i.e., the crack length may be measured accurately based on visual observations. A nylon insert with a thickness of 0.03 mm was placed at the midplane of each specimen to make an artificial starting defect. Then the specimens were precracked in an opening mode of 4–5 mm. The effect of precracking mode on the initiation toughness was investigated by Davidson et al. [30], Polaha et al. [31], and de Morais et al. [32]. They have found that in the case of mode-I precracking, the toughness may be expected to be lower in comparison with the mode-II precracking. Also, the toughness has a higher value when the crack is initiated directly from the insert, as shown in [31]. Thus, in the following, the presented results should

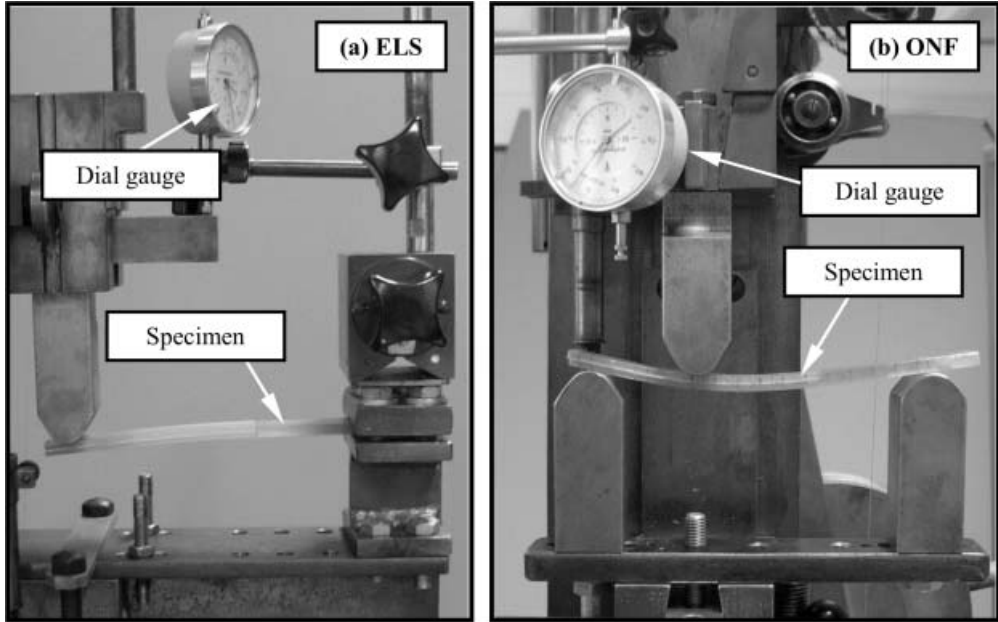


Figure 4. End-loaded split (a) and over-notched flexure (b) tests for mode-II interlaminar fracture.

be considered in the light of these establishments. The flexural modulus was determined from a three-point bending test using six uncracked specimens with a span length of 151 mm and a thickness of 6.1 mm. The experiment resulted in $E_{11} = 33$ GPa, additional properties were predicted by means of Niederstadt's [33] approximate rule of mixture, this way $E_{33} = 7.2$ GPa, $G_{13} = 3$ GPa, and $\nu_{13} = 0.27$ were obtained.

The fixtures for the ELS and ONF tests are illustrated in Figure 4. The tests were carried out using an Amsler testing machine under displacement control. The load–deflection data were measured, the latter was monitored by the dial gauge, shown in Figure 4(a) and (b). The distance between the load and the clamped cross section was $L = 150$ mm in the case of the ELS geometry. The full span length was $2L = 151$ mm for the ONF test, the position of the external load was $s = 47.5$ mm (refer to Figure 1). The contact regions above the supports were slightly roughened in order to prevent longitudinal sliding during the ONF test.

Two kinds of measurements were carried out. At the first stage, initiation tests were performed on both the configurations. In the case of the ELS test, the specimens with the following initial crack length values were prepared: 35, 40, 45, 50, 55, 60, 65, 70, 75, 80, 90, 100, 110, 120, 130, and 140 mm. This allowed for the determination of the initiation fracture properties in quite an extended ($0.23L \leq a \leq 0.93L$) crack length range. For the ONF test, the crack length range from 50 to 105 mm ($0.33 \cdot 2L \leq a \leq 0.69 \cdot 2L$) with 5 mm increment was investigated. If the initial crack length was higher than 105 mm, then we were unable to facilitate crack initiation, and large displacement of the specimens occurred. The specimens were tested to failure at the crack length of interest and the critical load and deflection were recorded.

At the second stage, propagation tests using six ONF specimens with $a_0 = 50$ mm initial crack length were performed. In this case, a millimeter scale was traced on the lateral sides

of the specimens, the crack length was measured visually by following the crack front on the upper surface of the specimens, and the position of the crack tip was marked. The compliance of the specimens was determined at each crack length. The reason for using only the ONF test for crack propagation is that in the case of the ELS configuration, the crack initiation was followed by large displacements. We were not able to control the crack propagation even in those crack lengths, where the stable crack propagation would have been expected.

Two methods were used for data reduction apart from the beam theory-based approach and the VCCT: the compliance calibration (CC) [34] and the direct beam theory approaches [8].

Compliance Calibration

In the case of the ELS test, the experimental compliance values were fit with a third-order polynomial of the form as in [34]:

$$C^{\text{ELS}} = C_{01} + ma^3, \quad (27)$$

where C_{01} and m were found by using least square fitting. The compliance of the ONF specimen may be written as [12]:

$$C^{\text{ONF}} = C_{02} + n(a - 2L)^3. \quad (28)$$

The coefficients C_{02} and n were determined in the same fashion. The SERR was calculated using Equation (18).

Direct Beam Theory

In this case, the flexural modulus of the specimens is eliminated. The relevant equations based on direct beam theory are:

$$G_{\text{II}}^{\text{ELS}} = \frac{9P\delta a^2}{2b(3a^3 - L^3)}, \quad (29)$$

$$G_{\text{II}}^{\text{ONF}} = \frac{9P\delta}{2b(2L - a)} \frac{1}{\theta}, \quad (30)$$

where

$$\theta = 1 + \frac{4a}{2L - a} + \frac{8aL}{(2L - a)^2} + \frac{16L^2a}{(2L - a)^3} + \frac{8Ls(s - 4L)}{(2L - a)^3}, \quad (31)$$

where P is the applied load and δ is the experimentally determined specimen displacement, respectively.

Crack Length Correction

The loading head and supports of our (non-standard) test fixture have relatively large radii (refer to Figure 4(a) and (b)). Figure 5(a) shows how the contact line between the loading head and the specimen changes as the load increases, and so, for example, the crack length becomes shorter. This fact should be considered in the data reduction. The corrections are calculated based on simple beam theory and the experimentally measured displacement at the point of load application.

For the ELS coupon, the end displacement and the derivative of the deflection based on simple beam theory are:

$$\delta = \frac{P(3a^{*3} + L^{*3})}{2bh^3 E_{11}}, \quad \phi = \frac{3P(3a^{*2} + L^{*2})}{4bh^3 E_{11}}. \quad (32)$$

On the basis of Figure 5(a), the corrected crack length and the specimen length are:

$$a = a^* - R \sin \phi \cong a^* - R \left(\phi - \frac{\phi^3}{3!} + \dots \right), \quad L = L^* - R \sin \phi \cong L^* - R \left(\phi - \frac{\phi^3}{3!} + \dots \right). \quad (33)$$

Combining the first and second expressions in Equation (32) one may obtain:

$$\phi = \chi \delta, \quad \chi = \frac{3(3a^{*2} + L^{*2})}{2(3a^{*3} + L^{*3})}. \quad (34)$$

Equation (33) can be rewritten as:

$$a \cong a^* - R_1 \left(\chi \delta - \frac{(\chi \delta)^3}{6} \right), \quad L \cong L^* - R_1 \left(\chi \delta - \frac{(\chi \delta)^3}{6} \right), \quad (35)$$

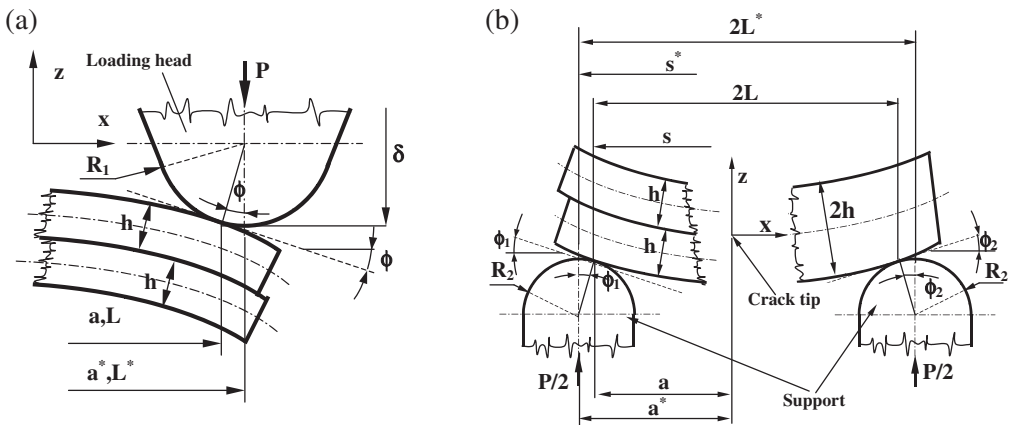


Figure 5. Correction of the ELS (a) and ONF (b) systems.

Note that in all the equations, a and a^* are the corrected, and the measured crack length, respectively, L and L^* are the corrected and the measured specimen length, respectively, and δ is the experimentally measured specimen displacement. The radius of the loading head is: $R_1 = 6$ mm.

A similar approach for the ONF specimen (Figure 5(b)) results in the following equations:

$$\begin{aligned}\chi_1 &= \frac{8L^{*3} + 3a^{*3} - 18L^*a^{*2} + 36a^*L^{*2} - 24s^*L^{*2} + 4L^*s^{*2}}{s^*(8L^{*3} + 3a^{*3} - 18L^*a^{*2} + 36a^*L^{*2} - 32s^*L^{*2} + 8L^*s^{*2})}, \\ \chi_2 &= \frac{4L^{*3} - 3a^{*3} + 9L^*a^{*2} - 4L^*s^{*2}}{s^*(8L^{*3} + 3a^{*3} - 18L^*a^{*2} + 36a^*L^{*2} - 32s^*L^{*2} + 8L^*s^{*2})}.\end{aligned}\quad (36)$$

The corrected parameters are:

$$a \cong a^* - R_2 \left(\chi_1 \delta - \frac{(\chi_1 \delta)^3}{6} \right), \quad s \cong s^* - R_2 \left(\chi_1 \delta - \frac{(\chi_1 \delta)^3}{6} \right), \quad (37)$$

$$2L \cong 2L^* - R_2 \left([\chi_1 + \chi_2] \delta - \frac{([\chi_1 + \chi_2] \delta)^3}{6} \right), \quad (38)$$

where s^* and s are the measured and the corrected position of the applied load from the left support, respectively and $R_2 = 8$ mm is the radius of the supports. Also, the FE models were constructed using the corrected geometrical parameters.

RESULTS AND DISCUSSION

Initiation Tests

LOAD AND DEFLECTION

The recorded load–displacement curves up to fracture initiation are illustrated in Figure 6. The response was essentially linear elastic, which confirms the application of LEFM. It is apparent that the critical load decreases with the initial crack length in the case of the ELS specimen. On the contrary, the ONF specimen requires higher load values for fracture initiation as the crack length increases. The range of the applied load is approximately three times higher in the ONF than in the ELS case. In spite of this, the ELS specimens suffered from large displacements, especially in the ranges of $a = 35$ – 60 mm, and 110 – 140 mm, as seen in Figure 6(a). During the ONF test, no large displacements were experienced in the mentioned crack length range, which is one of the greatest advantages of this setup.

COMPLIANCE AND STRAIN ENERGY RELEASE RATE

The compliance values calculated from the beam theory-based solution (Equations (17) and (20)) were compared with the results of the FE analysis. Tables 1 and 2 show the ratio between the results of the two solutions. The agreement between them was found to be excellent, which confirms the applicability of the analytical solutions.

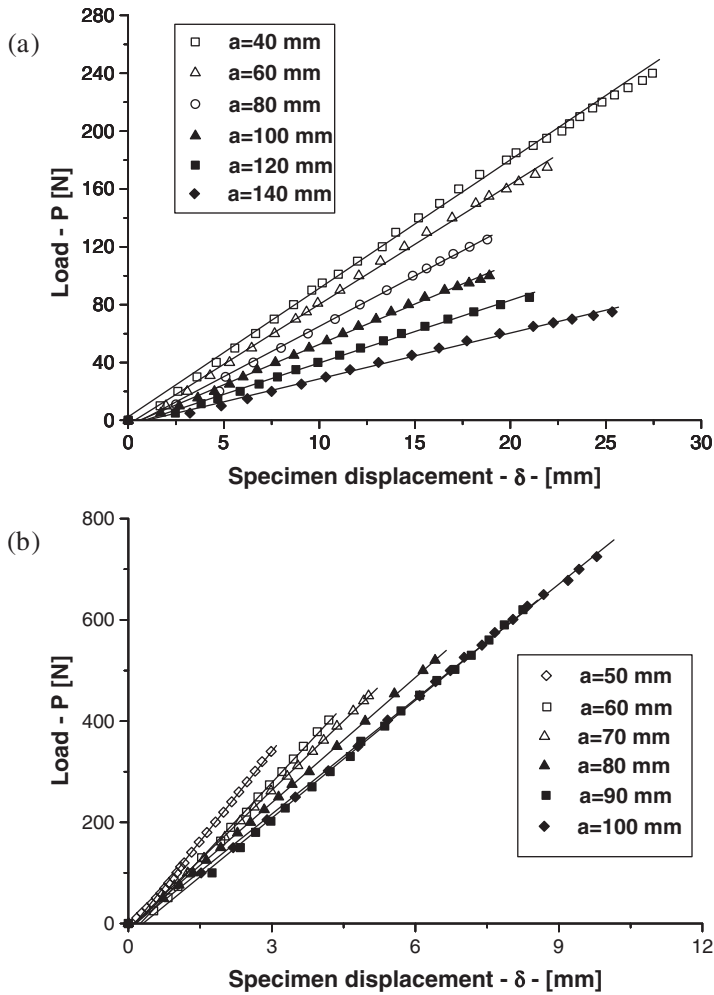


Figure 6. Load–displacement curves up to fracture initiation, ELS test (a) and ONF test (b).

Table 1. Comparison of the results by the FE and beam models, ELS specimen.

| a^* | 35 | 40 | 45 | 50 | 55 | 60 | 65 | 70 | 75 | 80 | 90 | 100 | 110 | 120 | 130 | 140 |
|-------------------|-------|-------|-------|-------|-------|-------|-------|-------|-------|-------|-------|-------|-------|-------|-------|-------|
| C_{FE}/C_{Beam} | 1.068 | 1.074 | 1.091 | 1.069 | 1.055 | 1.062 | 1.060 | 1.056 | 1.053 | 1.050 | 1.055 | 1.049 | 1.033 | 1.030 | 1.028 | 1.025 |

a^* —measured crack length; C_{FE} —compliance, plane strain FE model; and C_{Beam} —compliance, beam model, Equation (17).

Table 2. Comparison of the results by the FE and beam models, ONF specimen.

| a^* | 50 | 55 | 60 | 65 | 70 | 75 | 80 | 85 | 90 | 95 | 100 | 105 |
|-------------------|-------|-------|-------|-------|-------|-------|-------|-------|-------|-------|-------|-------|
| C_{FE}/C_{Beam} | 1.011 | 1.014 | 1.009 | 1.010 | 1.011 | 1.009 | 1.014 | 1.014 | 1.002 | 1.005 | 1.007 | 1.010 |

a^* —measured crack length; C_{FE} —compliance, plane strain FE model; C_{Beam} —compliance, beam model, Equation (20).

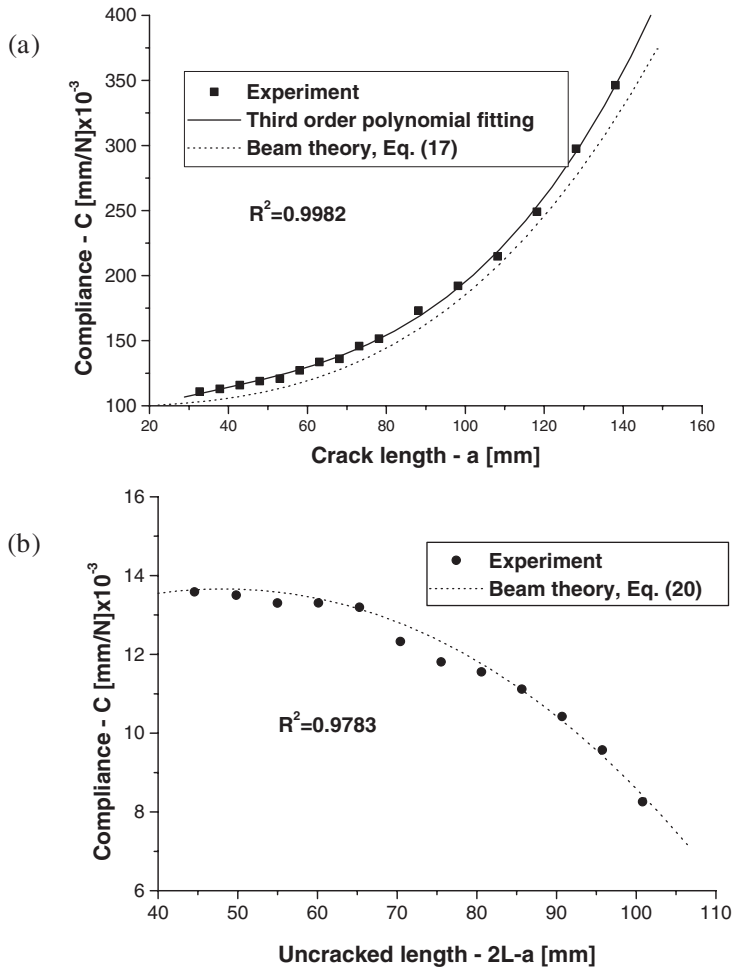


Figure 7. Measured and calculated compliance from initiation tests, ELS specimen (a) and ONF specimen (b).

The compliances determined based on initiation tests are plotted in Figure 7. For the ELS specimen, the advanced beam equation (Equation (17)) shows good agreement with the experimental points. The ONF test produces a somewhat unusual compliance curve. It is important to note that in this case, the characteristic distance is the length of the uncracked region. Otherwise, Equation (20) closely agrees with the experimental compliance values.

Four methods were used to calculate the strain energy release rate. Its values versus the crack length are illustrated in Figure 7. Each set of data points was fit with a third-order polynomial. For the ELS test, the CC method indicates a 713 J/m² plateau value, while the direct beam theory gives the value of 765 J/m². This means that there is a 7% difference between them. The analytical solution (Equation (19)) agrees well with the results of the CC and the VCCT methods; however, the latter provides slightly lower values. As a consequence, the four reduction schemes show good correlation in the case of the ELS coupon. From other perspectives, it is clear (Figure 8(a)) that the SERR

values depend on the crack length, but this is not serious. Figure 8(b) presents the SERR values from the ONF test as obtained by the various methods of data reduction. It seems that in this case, the CC method gives somewhat surprising results. The direct beam theory indicates a 790 J/m^2 steady-state value (which correlates well with the results of the ELS test), while the value of 540 J/m^2 was obtained by means of the CC method (31% difference). Both the analytical (Equation (21)) and numerical (VCCT) solutions show values, which are closer to the results of the direct beam theory. Therefore, we may assume that the application of the CC method is highly questionable in this case.

Propagation Tests

We have found that the ELS geometry was not suitable to investigate the crack propagation in the current material. The reason for that may be explained as follows. The ELS specimens suffered from relatively large displacements in order to overcome

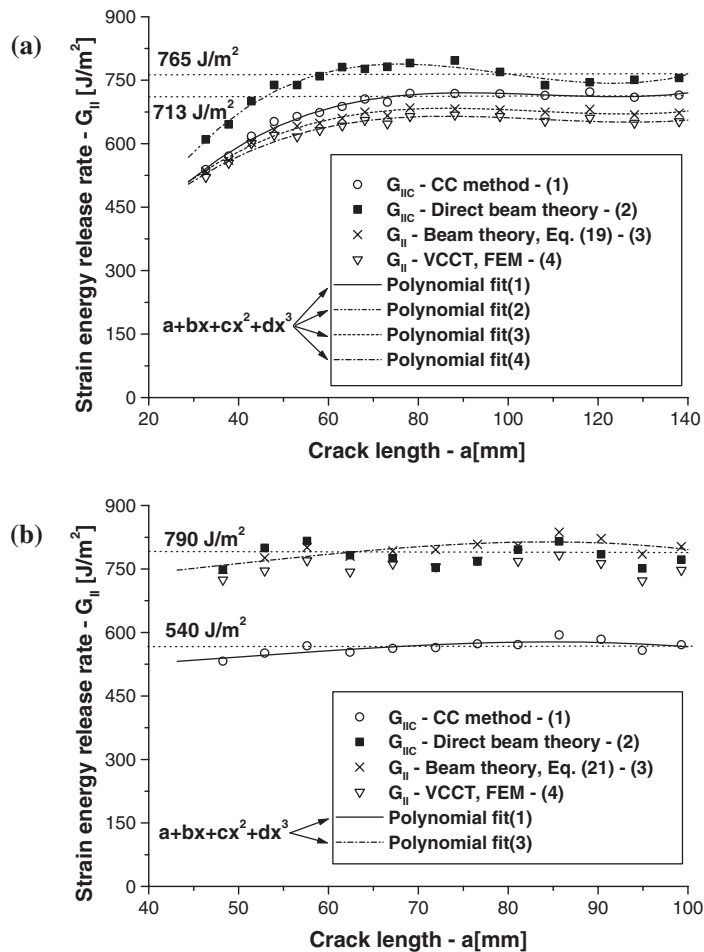


Figure 8. Values of the SERR from initiation tests, ELS (a) and ONF (b).

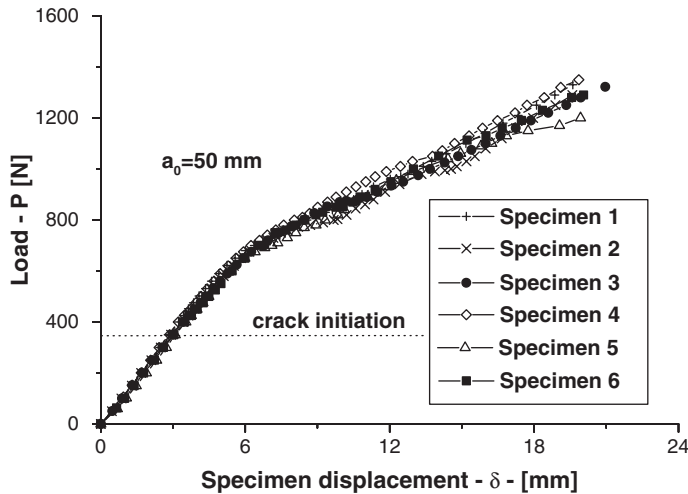


Figure 9. Load–displacement curves from ONF propagation tests.

the point of fracture initiation. To facilitate the crack propagation, larger displacements were required. After crack initiation, the crack seemed beyond control, i.e., the crack had reached the clamped end in a flash. This indicated that the stiffness of the system was not large enough for the ELS test. This may be supported by the large amount of experimental work performed, in general, on those composite materials, which exhibit high flexural modulus [8–10,12]. Thus, in the sequel, the attention is focused on the ONF test to measure the propagation toughness.

LOAD–DISPLACEMENT CURVES

The recorded load–displacement curves from the measurement of six ONF specimens are shown in Figure 9. It is noteworthy that the range of the applied load is about twice higher in comparison with that of the initiation tests (refer to Figure 6(b)). Crack initiation was observed always around 350–400 N.

COMPLIANCE AND FRACTURE RESISTANCE

The measured compliance values and the calculated curves are plotted in Figure 10 as obtained by the propagation test data of one specimen. A remarkable feature is that the experimentally measured compliance values somewhat differ from those obtained by the initiation tests (refer to Figure 7(b)). On the other hand, the beam theory-based solution (Equation (20)) does not match as well with the experimental values, as it does in the case of the initiation tests. The fiber bridging is one possible source of the mentioned discrepancy. During crack propagation, some of the fibers were pulled out, this caused the extensive fiber bridging between the crack faces. This feature increased the resistance to delamination, and consequently, a higher load value was required for the crack advance. Further work is required to clarify the discrepancy between the measured and calculated compliance.

Three reduction schemes were used to calculate the SERR. The results for two specimens are presented in Figure 11(a)–(c). The CC method shows that the value at which steady-state crack propagation occurred are 2670 and 2414 J/m², respectively. The data by

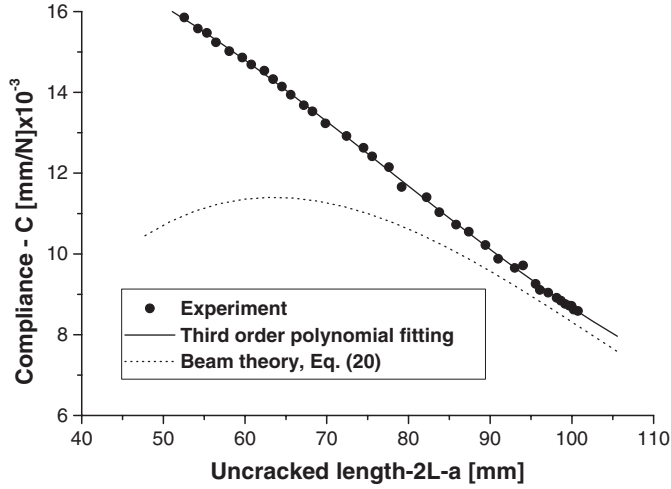


Figure 10. Measured and calculated compliance from the propagation test of one ONF specimen.

six specimens yielded a mean value of 2789 J/m^2 for the critical SERR. The plateau values were determined by using the asymptotic values of the fits in Figure 11. The relevant steady-state values are 3050 and 2589 J/m^2 (3121 J/m^2 mean value from six specimens) from the direct beam theory and 2893 and 2497 J/m^2 (2790 J/m^2 average value from six coupons) from the beam theory-based solution.

It should be kept in mind, that the CC method is the only data reduction technique, which considers the effect of fiber bridging. We have found that the CC technique is not recommended for the evaluation of initiation test data. It is important to note that in the case of propagation tests, the CC method showed good agreement with the analytical and the direct beam theory approaches. In spite of this, the result of the CC method is slightly doubtful. An experimental reduction scheme, which gives reliable results for initiation test and is able to account for the effect of fiber bridging would be useful. Further work is required to clarify these results.

Comparison with Published Results

For comparison, we provide some experimental results, which were previously published on similar systems. Ozdil et al. [15] investigated unidirectional glass–polyester ENF specimens with $a=32 \text{ mm}$ and $2L=100 \text{ mm}$. The value of $G_{\text{IIC}}=496 \pm 135 \text{ J/m}^2$ was obtained for the initiation energy release rate by using the simple beam theory solution. This is slightly less than those obtained by us (700 and 790 J/m^2); however, this value was obtained at a definite crack length, while in our experiments the extended ranges of crack length were investigated. Davies et al. [7] presented slightly higher G_{IIC} values for glass–epoxy ELS and ENF specimens as obtained by three different reduction techniques. For the ELS coupon, the critical (initiation) SERRs were within $1500\text{--}2000 \text{ J/m}^2$. In the case of the ENF test, they were $1400\text{--}1500 \text{ J/m}^2$. The significance of the employed data reduction was highlighted in the former work. Considering the propagation tests, the work by Davies et al. [6] may be referred to,

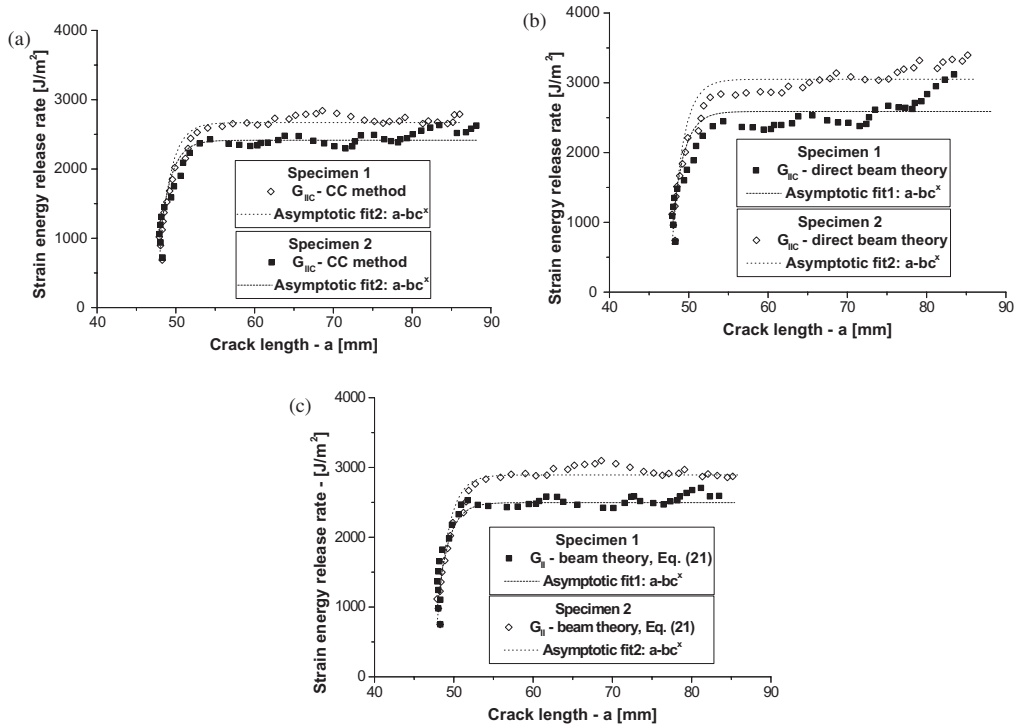


Figure 11. SERR against the crack length by different methods, ONF test. Compliance calibration (a); direct beam theory (b); and beam theory (c).

wherein they tested unidirectional glass–epoxy 4ENF specimens. For specimens with similar fiber volume fraction (52%) to that of our coupons and with $2L = 100$ mm, they measured $2013 \pm 135 \text{ J/m}^2$ initiation and $3040 \pm 450 \text{ J/m}^2$ propagation toughness in the range of $a = 47\text{--}76$ mm. These values are higher in comparison with our results; however, the R-curve followed a similar trend as found by us in Figure 11(a)–(c).

CONCLUSIONS

The mode-II interlaminar fracture in glass–polyester end-loaded split and over-notched flexure specimens were investigated from the theoretical and experimental points of view. Closed-form solutions were developed for the compliance and the strain energy release rate of the mentioned delamination coupons. The experiments and the developed finite element models validated the analytical solution. The experimental data were reduced by four methods in the case of the initiation tests. It was found that the compliance calibration method gives misleading results in the case of the ONF specimens. Consequently, the application of the CC method is not recommended. All the other solutions were in good agreement in both the test coupons.

The ONF specimen was used as a candidate to measure the propagation toughness. This test was found to be relatively easy to perform and the crack propagation was easy to control. In the light of these establishments, we may conclude that the ONF test

is an efficient tool to obtain the mode-II strain energy release rate of composite materials with low flexural modulus. The propagation test data were evaluated by three different methods: exact beam theory, compliance calibration, and direct beam theory. In each case, a clear plateau value was reached as the crack advanced. It is noteworthy that direct beam theory indicated the highest plateau value (3121 J/m^2), while the compliance calibration and exact beam theory provided identical result (2789 against 2790 J/m^2). This indicates the applicability of the present beam equations for data reduction.

The relatively high value of the mode-II toughness was supported by previous experiments carried out on similar type of composite materials.

ACKNOWLEDGMENTS

This research work was supported by the fund OTKA T037324. We wish to thank Barry D. Davidson for providing [29–31], Alfredo Balacó de Morais for [7,32], and Pizhong Qiao for [14]. The first author is grateful to his father for manufacturing the experimental tools. The first author also thanks Pál Varga for improving the English grammar and syntax.

REFERENCES

1. Schuecker, C. and Davidson, B.D. (2000). Evaluation of the Accuracy of the Four-point Bend End-notched Flexure Test for Mode II Delamination Toughness Determination, *Composites Science and Technology*, **60**: 2137–2146.
2. Todo, M., Takamura, T. and Takahashi, K. (1999). Mode II Interlaminar Fracture Behavior of Fiber Reinforced Polyamide Composites Under Static and Dynamic Loading Conditions, *Journal of Reinforced Plastics and Composites*, **18**: 1415–1427.
3. Tsai, J.L., Guo, C. and Sun, C.T. (2001). Dynamic Delamination Fracture Toughness in Unidirectional Polymeric Composites, *Composites Science and Technology*, **61**: 87–94.
4. Stevanovic, D., Jar, P.-Y.B., Kalyanasundaram, S. and Lowe, A. (2000). On Crack-initiation Conditions for Mode I and Mode II Delamination Testing of Composite Materials, *Composite Science and Technology*, **60**: 1879–1887.
5. Aksoy, A. and Carlsson, L.A. (1992). Interlaminar Shear Fracture of Interleaved Graphite/epoxy Composites, *Composites Science and Technology*, **43**: 55–69.
6. Davies, P., Casari, P. and Carlsson, L.A. (2005). Influence of Fiber Volume Fraction On Mode II Interlaminar Fracture Toughness of Glass/epoxy Using the 4ENF Specimen, *Composites Science and Technology*, **65**: 295–300.
7. Davies, P., Ducept, F., Brunner, A.J., Blackman, B.R.K. and de Morais, A.B. (1996). Development of a Standard Mode II Shear Fracture Test Procedure, In: *Proceedings of the 7th European Conference on Composite Materials (ECCM-7)*, London, May 1996, Vol. 2, pp. 9–15.
8. Hashemi, S., Kinloch, J. and Williams, J.G. (1990). The Effects of Geometry, Rate and Temperature on Mode I, Mode II and Mixed-mode I/II Interlaminar Fracture Toughness of Carbon-fibre/Poly(Ether-Ether Ketone) Composites, *Journal of Composite Materials*, **24**: 918–956.
9. Hashemi, S., Kinloch, J. and Williams, J.G. (1990). Mechanics and Mechanisms of Delamination in a Poly(Ether Sulphone)-Fibre Composites, *Composites Science and Technology*, **37**: 429–462.

10. Wang, H. and Vu-Khanh, T. (1996). Use of End-loaded-split (ELS) Test to Study Stable Fracture Behaviour of Composites Under Mode-II Loading, *Composite Structures*, **36**: 71–79.
11. Tanaka, K., Yuasa, T. and Katsura, K. (1998). Continuous Mode II Interlaminar Fracture Toughness Measurement by Over Notched Flexure Test, In: *Proceedings of the 4th European Conference on Composites: Testing and Standardization*, pp. 171–179.
12. Wang, W.-X., Takao, Y. and Nakata, M. (2003). Effects of Friction on the Measurement of the Mode II Interlaminar Fracture Toughness of Composite Laminates, In: *Proceedings of the 14th International Conference on Composite Materials*, San Diego, California, USA, July 14–18.
13. Qiao, P., Wang, J. and Davalos, J.F. (2003). Analysis of Tapered ENF Specimen and Characterization of Bonded Interface Fracture Under Mode-II Loading, *International Journal of Solids and Structures*, **40**: 1865–1884, *Corrigendum*, **40**: 4091.
14. Wang, J. and Qiao, P. (2003). Fracture Toughness of Wood-wood and Wood-FRP Bonded Interfaces Under Mode-II Loading, *Journal of Composite Materials*, **37**: 875–898.
15. Ozdil, F., Carlsson, L.A. and Davies, P. (1998). Beam Analysis of Angle-ply Laminate End-notched Flexure Specimens, *Composites Science and Technology*, **58**: 1929–1938.
16. Carlsson, L.A., Gillespie, J.W. and Pipes, R.B. (1986). On the Analysis and Design of the End Notched Flexure (ENF) Specimen for Mode II Testing, *Journal of Composite Materials*, **20**: 594–604.
17. Olsson, R. (1992). A Simplified Improved Beam Analysis of the DCB Specimen, *Composites Science and Technology*, **43**: 329–338.
18. Ozdil, F. and Carlsson, L.A. (1999). Beam Analysis of Angle-ply Laminate DCB Specimens, *Composites Science and Technology*, **59**: 305–315.
19. Chatterje, S.N. (1991). Analysis of Test Specimens for Interlaminar Mode II Fracture Toughness, Part I. Elastic Laminates, *Journal of Composite Materials*, **25**: 470–493.
20. Ding, W. and Kortschot, M.T. (1999). A Simplified Beam Analysis of the End Notched Flexure Mode II Delamination Specimen, *Composite Structures*, **45**: 271–278.
21. Wang, J. and Qiao, P. (2004). Novel Beam Analysis of the End Notched Flexure Specimen for Mode-II Fracture, *Engineering Fracture Mechanics*, **71**: 219–231.
22. Wang, J. and Qiao, P. (2004). Interface Crack Between two Shear Deformable Elastic Layers, *Journal of the Mechanics and Physics of Solids*, **52**(4): 891–905.
23. Qiao, P. and Wang, J. (2004). Mechanics and Fracture of Crack-tip Deformable Bimaterial Interface, *International Journal of Solids and Structures*, **41**(26): 7423–7444.
24. Wang, Y. and Williams, J.G. (1992). Corrections for Mode II Fracture Toughness Specimens of Composite Materials, *Composites Science and Technology*, **43**: 251–256.
25. Bao, G., Ho, S., Suo, Z. and Fan, B. (1992). The Role of Material Orthotropy in Fracture Specimens for Composites, *International Journal of Solids and Structures*, **29**: 1105–1116.
26. Davies, P., Kausch, H.H., Williams, J.G., Kinloch, A.J., Charalambides, M.N., Pavan, A., Moore, D.R., Prediger, R., Robinson, I., Burgoyne, N., Friedrich, K., Wittich, H., Rebelo, C.A., Torres Marques, A., Ramsteiner, F., Melve, B., Fischer, M., Roux, N., Martin, D., Czarnocki, P., Neville, D., Vepoest, I., Goffaux, B., Lee, R., Walls, K., Trigwell, N., Partridge, I.K., Jaussaud, J., Andersen, S., Giraud, Y., Hale, G. and McGrath, G. (1992). Round-robin Interlaminar Fracture Testing of Carbon-fibre-reinforced Epoxy and PEEK Composites, *Composites Science and Technology*, **43**: 129–136.
27. Schön, J. (2000). Coefficient of Friction of Composite Delamination Surfaces, *Wear*, **237**: 77–89.
28. Yang, Z. and Sun, C.T. (2000). Interlaminar Fracture Toughness of a Graphite/epoxy Multidirectional Composite, *Journal of Engineering Materials and Technology*, **122**: 428–433.
29. Davidson, B.D. and Sundararaman, V. (1996). A Single Leg Bending Test for Interfacial Fracture Toughness Determination, *International Journal of Fracture*, **78**: 193–210.
30. Davidson, B.D. and Koudela, K.L. (1999). Influence of the Mode Mix of Pre-cracking on the Delamination Toughness of Laminated Composites, *Journal of Reinforced Plastics and Composites*, **18**: 1408–1414.

31. Polaha, J.J., Davidson, B.D., Hudson, R.C. and Pieracci, A. (1996). Effects of Mode Ratio, Ply Orientation and Precracking on the Delamination Toughness of a Laminated Composite, *Journal of Reinforced Plastics and Composites*, **15**: 141–173.
32. de Morais, A.B., Rebelo C.C., de Castro, P.M.S.T., Marques, T. and Davies, P. (2004). Interlaminar Fracture Studies in Portugal: Past, Present and Future, *Fatigue and Fracture of Engineering Materials and Structures*, **27**: 767–773.
33. Thamm, F. (1985). *Strength of Plastic Materials II*. Budapest Coursebook Publisher, Budapest (in hungarian).
34. Dahlen, C. and Springer, G.S. (1994). Delamination Growth in Composites Under Cyclic Loads, *Journal of Composite Materials*, **28**: 732–781.